Membrane potential mediates an ancient mechano-transduction mechanism for multi-cellular homeostasis

Avik Mukherjee*, Yanqing Huang*, Jens Elgeti, Seungeun Oh, Anjali Rebecca Neliat, Janik Schüttler, Nina Catherine Benites, Xili Liu, Mihail Barboiu, Hugo Stocker, Marc W. Kirschner, Markus Basan[#]

[#] Correspondence: markus@hms.harvard.edu , *equal contribution

Membrane potential is a property of all living cells[1]. However, its physiological role in non-excitable cells is poorly understood. Resting membrane potential is typically considered fixed for a given cell type and under tight homeostatic control[2], akin to body temperature in mammals. Contrary to this widely accepted paradigm, we found that membrane potential is a dynamic property that directly reflects tissue density and mechanical forces acting on the cell. Serving as a quasi-instantaneous, global readout of density and mechanical pressure, membrane potential is integrated with signal transduction networks by affecting the conformation and clustering of proteins in the membrane[3,4], as well as the transmembrane flux of key signaling ions[5,6]. Indeed, we show that important mechano-sensing pathways, YAP, Jnk and p38[7–12][13][14], are directly controlled by membrane potential. We further show that mechano-transduction via membrane potential plays a critical role in the homeostasis of epithelial tissues, setting tissue density by controlling proliferation and cell extrusion of cells. Moreover, a wave of depolarization triggered by mechanical stretch enhances the speed of wound healing. Mechano-transduction via membrane potential likely constitutes an ancient homeostatic mechanism in multi-cellular organisms, potentially serving as a steppingstone for the evolution of excitable tissues and neuronal mechano-sensing. The breakdown of membrane potential mediated homeostatic regulation may contribute to tumor growth.

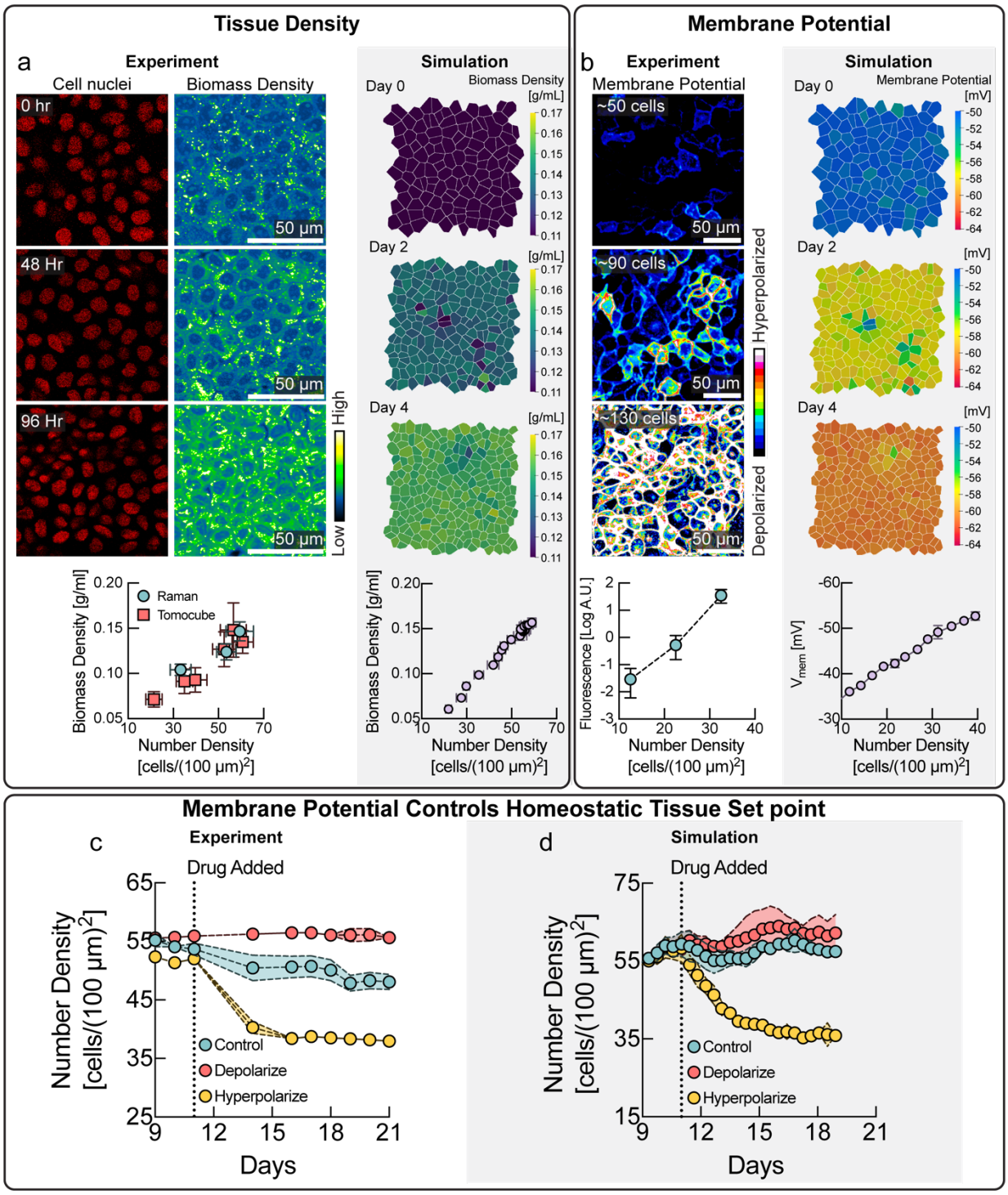

Figure 1: Membrane potential is a sensor and regulator of tissue density. a*, Madin-Darby Canine Kidney (MDCK) cells imaged for 4 consecutive days after confluence with increasing cell number density. Left row of images shows number of cell nuclei and middle row of images shows cellular biomass density (in units of g/ml) measured via Normalized Stimulated Raman*

Spectroscopy (NoRI). Plot below show cellular biomass density quantified as a function of cell number density in the tissue. Biomass density was measured using two different experimental methods (NoRI imaging and holotomographic microscopy). Right row of images are snapshots of the tissue simulation with biomass density represented by the color code. Plot below is corresponding biomass density as a function of cell number density from the tissue simulation. ***b,*** *Left row of images shows MDCK cells, stably expressing Voltron biosensor. An increase in fluorescence intensity indicates hyperpolarization of cellular membrane potential. Cells show progressive hyperpolarization as a function of increasing cell density. Plot below is a quantification of reporter readout of membrane potential as a function of tissue density. Right row of images are snapshots of the tissue simulation (same as in panel a) with membrane potential represented by the color code. Plot below shows corresponding quantification of membrane potential as a function of tissue density in the simulation.* ***c,*** *Left plot is a quantification of cell number density for MDCK cells grown to maximum tissue density and treated with depolarizing and hyperpolarizing drugs (dashed line) as a function of time. Steady-state (homeostatic) tissue density can be modulated by membrane potential. Depolarization results in higher tissue density (red) as compared to the control without drugs (blue). Conversely, hyperpolarization results in a substantially lower tissue density (yellow). Right plot shows corresponding results from the tissue simulation. The mechanisms of different depolarizing and hyperpolarizing drugs were implemented in the tissue simulation via the mechano-electro-osmotic model. Just as observed experimentally, depolarizing drugs result in a higher homeostatic tissue density (red), whereas hyperpolarizing drugs result in a decrease of higher homeostatic tissue density (yellow), as compared to the unperturbed tissue (blue).*

Epithelia constitute a critical step in the evolution of multi-cellular organisms that shaped the complexity and diversity of metazoan phenotypic landscape[15]. Constituting the majority of mammalian tissues and performing a range of essential physiological functions, ranging from barriers to the topological exterior to nutrient uptake, epithelia not only need to tightly regulate cell number and growth, but the breakdown of these controls can lead to tumorigenesis. To better understand how epithelial cells achieve homeostasis in confluent tissues, we used normalized Raman imaging (NoRI)[16] to quantify intracellular biomass of epithelial MDCK monolayers at different levels of confluence (Fig. 1a, Fig. S1). Remarkably, rather than remaining constant, as might naively be expected, we observed a striking increase of intracellular biomass density with increasing number of cells. We confirmed this observation with a second independent experimental technique, based on laser interferometry, also referred to as holo-tomographic microscopy (Tomocube) (Fig. 1a, red squares & Fig. S2)[17,18].

We wanted to know which other physiological changes coincided with this change of biomass density. Inspired by a classic physical phenomenon from equilibrium thermodynamics[19], we wanted to know if changes in biomass density were reflected in changes of membrane potential. Using a hybrid voltage-indicator Voltron [20], we quantified resting membrane potential in MDCK cells for increasing cell number and biomass density. Strikingly, we found that MDCK cells became increasingly hyperpolarized with increasing cell number (Fig. 1b). This finding is surprising because membrane potential is typically considered to be constant for a given cell type and under tight homeostatic control. We realized that this finding in MDCK cells was consistent with early micropipette-based measurements of resting membrane potential in CHO cells as they reached different levels confluence[21] (Fig. S3a, b), as well as measurements in different regions of

the tissue colony (Fig. S2d). The mechanistic origin of these early observations was never elucidated. We hypothesized that just like in MDCK cells, these changes in membrane potential might correlate with changes in cellular biomass density. Indeed, using NoRI imaging, we confirmed that in CHO cells, changes in membrane potential were accompanied by corresponding changes in cellular biomass density (Fig. S3), with denser cell being more negatively polarized.

The tight correlation of tissue density and membrane potential suggested that these physiological variables could be directly coupled. To test the causality of this relationship, we applied external osmotic pressure to compress cells and artificially increase their biomass density. Indeed, using a different ratiometric biosensor and a different membrane potential dye, we confirmed that both CHO cells and MDCK cells were hyperpolarized by osmotic compression (Fig. S4), suggesting that changes in membrane potential are indeed downstream of changes in biomass density.

Based on these observations, we hypothesized that membrane potential could be directly involved in regulating tissue density. To test this hypothesis, we grew MDCK cells to maximum density and then applied either depolarizing or hyperpolarizing drugs to the tissue culture. Remarkably, cells in depolarizing conditions (Fig. 1c, red symbols) maintained a significantly higher cell number density, than cells grown in the absence of drugs (Fig. 1c, cyan symbols) and we found this effect to be independent of the depolarizing drug used (Fig. S5). Conversely, cell number density in hyperpolarizing conditions dropped and then plateaued at a substantially lower level (Fig. 1c, yellow) than in the tissues grown in the absence of drugs (Fig. 1c, cyan). This steady-state cell number density could be modulated continuously with the dose of the hyperpolarizing drug (Fig. S4), consistent with a regulatory role of membrane potential in controlling tissue density. We also confirmed that the increase in cell number density induced by depolarization was reflected in an increase of cellular biomass density (Fig. S6).

To understand the origin of the remarkable correlation between tissue density and membrane potential that we observed, we built a biophysical mathematical model of ion homeostasis. Classical models of membrane potential do not consider mechanical forces[2,22]. However, membrane potential is intimately coupled to osmotic pressure of the cytoplasm and the balance of charged ions and macromolecules inside the cell. As illustrated in Box 1 (top), an imaginary cell resists external forces compressing it, via osmotic pressure resulting from an increased concentration of ions in the cytoplasm. However, this results in a steeper ion concentration gradient across the plasma membrane resulting in a larger efflux of ions. A buildup of membrane potential due to charged biomolecules inside the cell counteracts this diffusive efflux, retaining an elevated intracellular ion concentration to counteract the external pressure. Based only on elementary conservation laws, including active ion transport, but assuming no active biological regulation, we found that resting membrane potential naturally reflects osmotic pressure of the cytoplasm and the corresponding intracellular biomass density (see Box 1 & Supplementary Note 1). Thus, with a constant expression ratio of ion transporters and channels, membrane potential constitutes a cell size independent readout of total mechanical pressure on the cell and the corresponding cytoplasmic biomass density. We incorporated this mechano-electro-osmotic model, calibrated with physiological parameters, into a mechanical simulation of a mono-layered epithelium (Supplementary Note 2).

For cells working together in a multicellular tissue, it is crucial to determine the amount of space in the tissue to quickly close wounds and to prevent tumorous overgrowth. Membrane potential provides cells in the tissue with a quasi-instantaneous readout tissue density and mechanical constraints for regulation of tissue homeostasis (Fig. 1c). Because the coupling between mechanics, density and membrane potential requires no active regulation and is present even at thermodynamic equilibrium, we hypothesize that regulation via membrane potential could be one of the earliest homeostatic mechanisms in multi-cellular organisms. To test the idea that tissues can achieve homeostasis using only membrane potential as a readout, we implemented membrane potential as the sole regulator of biosynthesis and apoptosis in our simulation (see Supplementary Note 2 for details of implementation).

Indeed, the mechano-electro-osmotic model combined with the tissue simulation successfully recapitulated our experimental observations, including an increase in biomass density with cell number density (Fig. 1a, right side) and corresponding changes in membrane potential (Fig. 1b, right side). Moreover, implementing the effect of different depolarizing and hyperpolarizing drugs, the model recapitulated the observed changes in steady-state tissue density (Fig. 1c, right side). The effect of these drugs can be understood intuitively: Cells perceive mild depolarization as a state of low confluence and continue to grow to an excess density (Fig. 1c, red circles). Conversely, hyperpolarization by drugs leads to a lower homeostatic tissue density because cells interpret hyperpolarization as excess tissue density and arrest their growth prematurely.

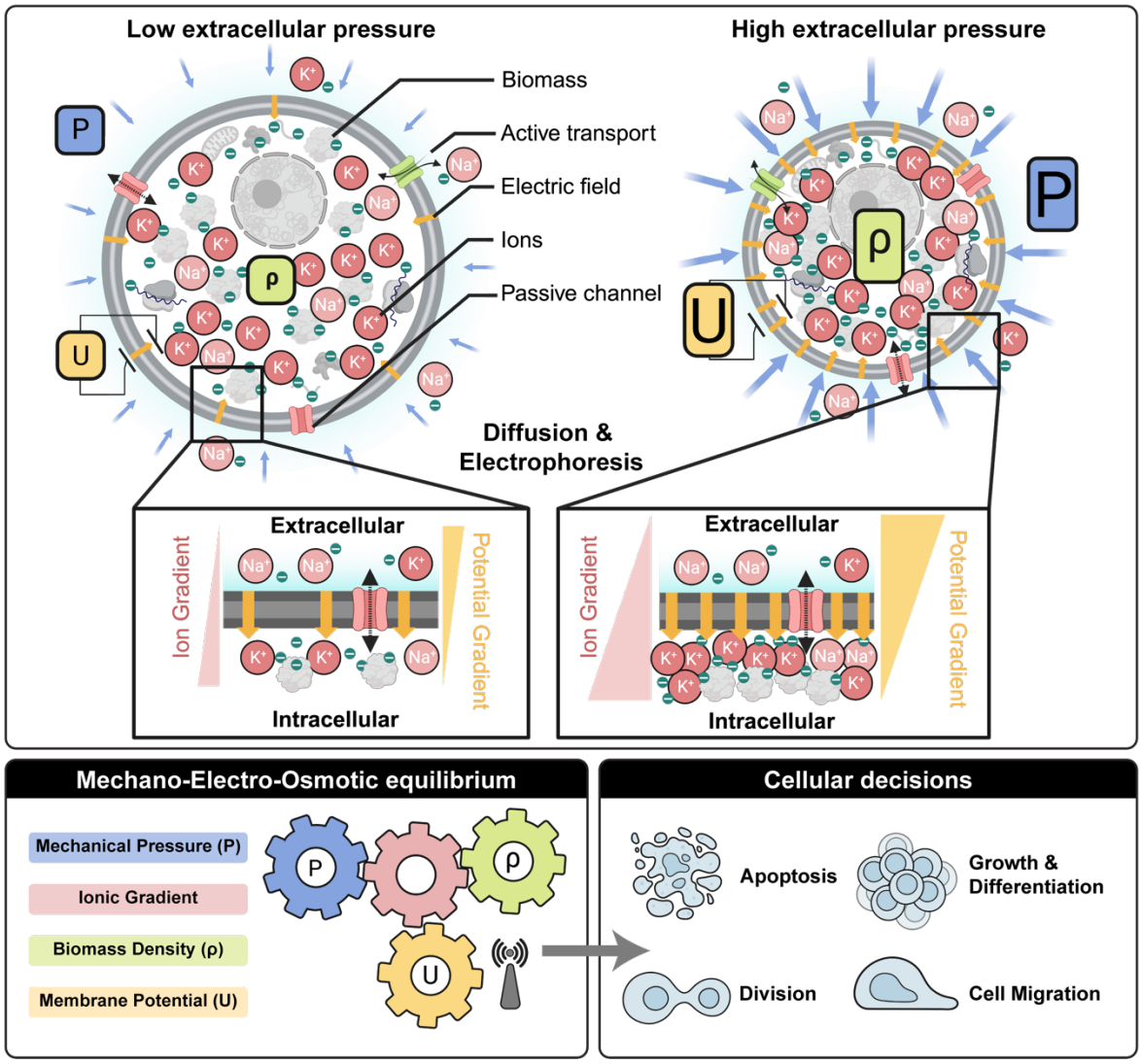

Box 1: Mechano-electro-osmotic model. Top: *The model combines three elementary conservation laws: Flux balance across the plasma membrane, mechanical force balance, and charge balance. Left-hand side illustrates a cell under low mechanical pressure and the right-hand side a corresponding cell under high mechanical pressure. Cellular biomass like protein and RNA carries a net negative charge. Cells resist compression of their volume via cytoplasmic osmotic pressure that counteracts and balances external forces (force balance). This osmotic pressure originates from an intracellular concentration of counterions that are attracted to balance negatively charged macromolecules (charge balance). As illustrated on the right-hand side, higher mechanical pressure acting in the cell is thus balanced by a higher concentration of counterions. Higher intracellular ion concentrations result in steeper concentration gradients across the membrane, as illustrated in the right inset. With constant ion channel abundances, a steeper concentration gradient across the membrane results in an augmented diffusive efflux of ions (Fick's law). With constant active ion transport flux (sodium-potassium-ATPase), this increased diffusive ion efflux results in a buildup of net negative charge in the cytoplasm and a corresponding membrane potential that counteracts the diffusive efflux of positively charged ions until flux is achieved (flux balance for each ion species).* ***Bottom:*** *A one-to-one correspondence between*

mechanical pressure, cytoplasmic biomass density and membrane potential emerges from the mechano-electro-osmotic equilibrium illustrated in the top panel. Crucial physiological properties like total biomass in relation to available space or mechanical and spatial constraints on the entire cell are difficult for cells to assess and integrate from individual molecular players. Membrane potential, on the other hand, provides an instantaneous, global readout of these physiological variables. We hypothesize that membrane potential is therefore the ideal starting point for signal transduction to control cellular decisions like growth, apoptosis, and cell motility to achieve tissue homeostasis.

The mechano-electro-osmotic model (Box 1) predicts that mechanical forces should be directly reflected in membrane potential. To test this prediction, we wanted to impose external mechanical perturbations on the tissue and measure the response of membrane potential. One elegant method, pioneered by the Rosenblatt lab, is to culture epithelial cells on an elastic membrane that can be stretched or de-stretched mechanically, thereby stretching, or compressing the tissue itself[21,23] (Fig. 2a). We cultured MDCK cells on such a stretchable PDMS membrane and waited till cells reached maximum number density. The voltage sensitive dye FluoVolt is ideally suited to image changes in membrane potential on short timescales and fluorescence intensity conveniently increases with depolarization[24]. Indeed, stretching the MDCK monolayer resulted in depolarization (Fig. 2a,b, quantified in panel c), consistent with simulation prediction (Fig. 2d). To check if this change in membrane potential was reversible on short timescales when we de-stretched the membrane, we used a different voltage indicator (DiSBAC2(3)[25]). Indeed, reducing the stretch of the PDMS membrane quickly led to repolarization of membrane potential (Fig. 2e,f), just as predicted by the simulation (Fig. 2g). According to the model, depolarization upon stretch is caused by a drop in cellular biomass density due to an increased cell volume, rather than tension in the plasma membrane or changes in cell-cell adhesion. Therefore, using NORI imaging, we quantified biomass density of the confluent monolayer just before the stretch and immediately after a 20% uniaxial stretch, and then again after overnight cultivation (Fig. 2h,i). Just as expected from the tissue simulation (Fig. 2j), we found that stretching resulted in a significant drop in biomass density and stretching induced biomass production and proliferation, as biomass density and cell number recovered to their initial level overnight. Conversely, we also confirmed that de-stretching the PDMS membrane resulted in an increase of cellular biomass density after overnight recovery (Fig. S7).

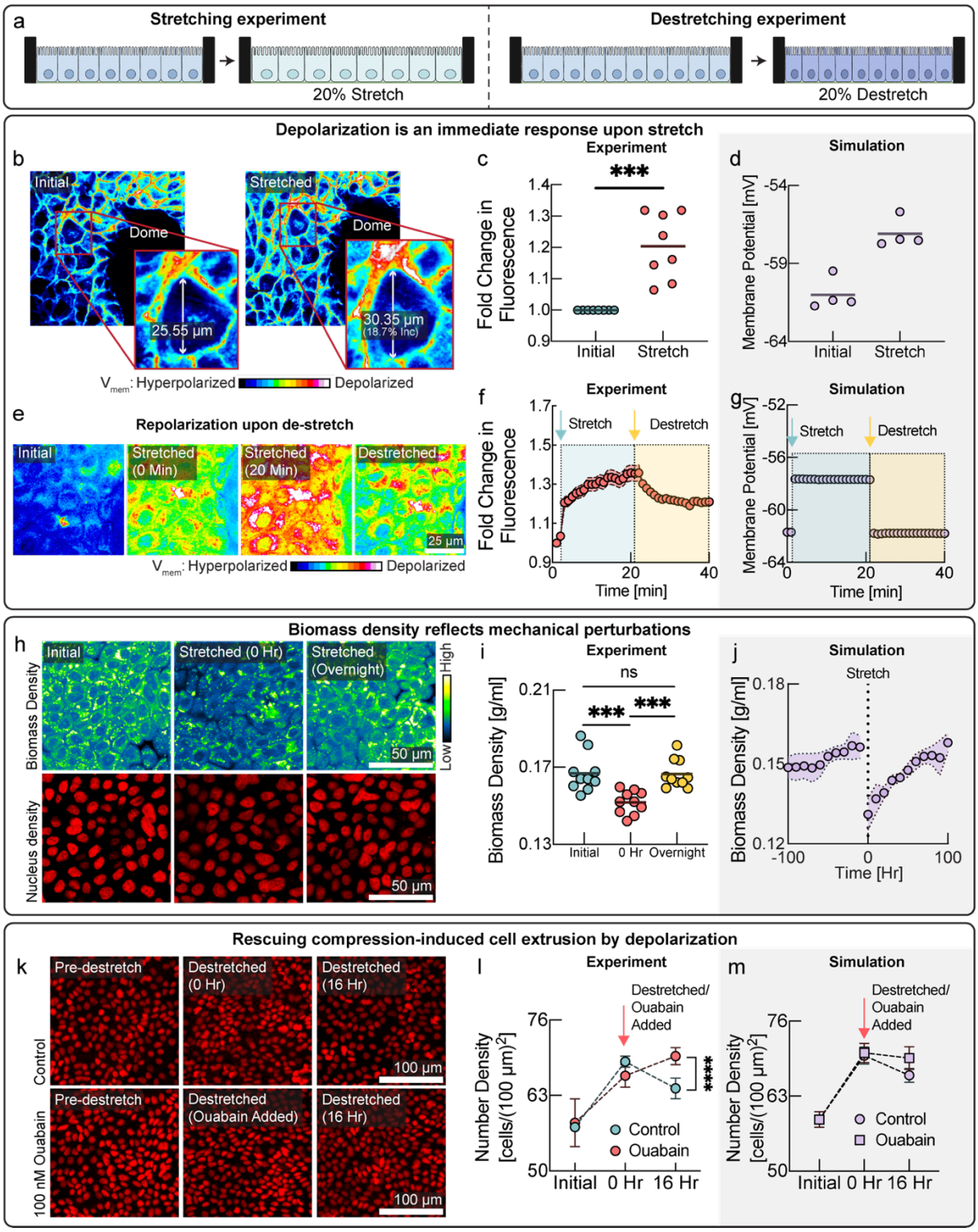

Figure 2: Cells detect and respond to mechanical forces via membrane potential. a, *Schematic diagram depicting the experimental design with cells on stretchable membrane. In one case, cells were grown to confluence and then 20% uniaxial stretch was applied (left panel) or cells and grown to confluence on a pre-stretched membrane, and then the stretch was released to induce*

compression (right panel). ***b,*** *Cells in a confluent monolayer depolarize rapidly on application of uniaxial stretch. Cells imaged in the presence of the membrane potential dye (Fluo-Volt), where an increase in fluorescence intensity indicates depolarization of membrane potential. Callout shows the increase in cellular area on stretching. Length was measured in the direction of stretch.* ***c,*** *Plot of fluorescence intensity (increase representing depolarization of membrane potential) on uniaxial stretching similar to panel b.* ***d,*** *Membrane potential predicted by the tissue simulation upon a 20% uniaxial stretch.* ***e,*** *Reversibility of membrane potential change on stretching and de-stretching using a different membrane potential indicator. Cells were grown to confluence on a stretchable PDMS membrane and loaded with membrane potential sensitive dye (DiSBAC2(3)). A 20% uni-axial stretch was applied (20%). Increase in fluorescence intensity represents depolarization on stretching. After the membrane was de-stretched, fluorescence intensity decreased quickly, indicating repolarization as compared to the stretched depolarized state. Note that for technical reasons, we cannot de-stretch back to exact same initial point.* ***f,*** *Quantification of reversibility of membrane potential on stretching and de-stretching. Increase in fluorescence intensity indicates depolarization, whereas decrease indicates hyperpolarization. Cyan arrow indicates the timepoint of stretch. Yellow arrow represents timepoint of de-stretch. Fast reversibility of depolarization of membrane potential rules out changes in permeability due to membrane stretch as the cause of depolarization.* ***g,*** *Corresponding tissue simulation predicting depolarization and repolarization upon stretch and de-stretch.* ***h****, Response of cellular biomass to tissue stretch, measured by NORI imaging. Biomass density of the confluent epithelial monolayer drops with uni-axial stretch. Biomass density recovers to the initial biomass density level overnight.* ***i,*** *Quantification of biomass density via NoRI imaging from same experiments as panel h.* ***j,*** *Tissue simulation recapitulates the drop of biomass density upon stretch and overnight recovery due to biomass production.* ***k,*** *Tissue crowding was induced by de-stretching of the PDMS membrane (top images). After 16h a significant number of cells had been eliminated, consistent with previous studies*[21,23]*. We show here that cells can be rescued from extrusion upon de-stretch and retained at a higher tissue density by mild-depolarization (bottom images).* ***l,*** *Quantification of cell number in same experiments as panel k. Depolarization leads to cell being retained in the tissue at a significantly higher cell number density than the control (red vs cyan data points).* ***m,*** *Tissue simulation recapitulates cell elimination after compression and rescue from elimination by depolarizing drugs.*

We wanted to directly test the potential role of membrane potential in regulating the response of cells to mechanical perturbations. Therefore, we grew MDCK cells on pre-stretched membranes to high cell density and then decreased the stretch to induce cell crowding and compression of the tissue (Fig. 2k). Cell extrusion in response to tissue compression is well established, as demonstrated by elegant experiments from the Rosenblatt lab [21,23]. If membrane potential hyperpolarization plays a role cell elimination in response to mechanical compression, it should be possible to retain a higher cell number density by depolarizing the tissue. Indeed, in the presence depolarizing drugs, cells maintained a significantly higher cell number density after the tissue was compressed (Fig. 2k, and 2l red circles) than control cells (Fig. 2k, and 2l blue circles). The observed experimental dynamics are consistent with our model and could be recapitulated with the tissue simulation (Fig. 2m). In a separate experiment, we induced crowding while cells were still in growth phase and observed the same increase of steady-state cell number density when cells were treated with a different depolarizing drug, TCT (Fig. S8).

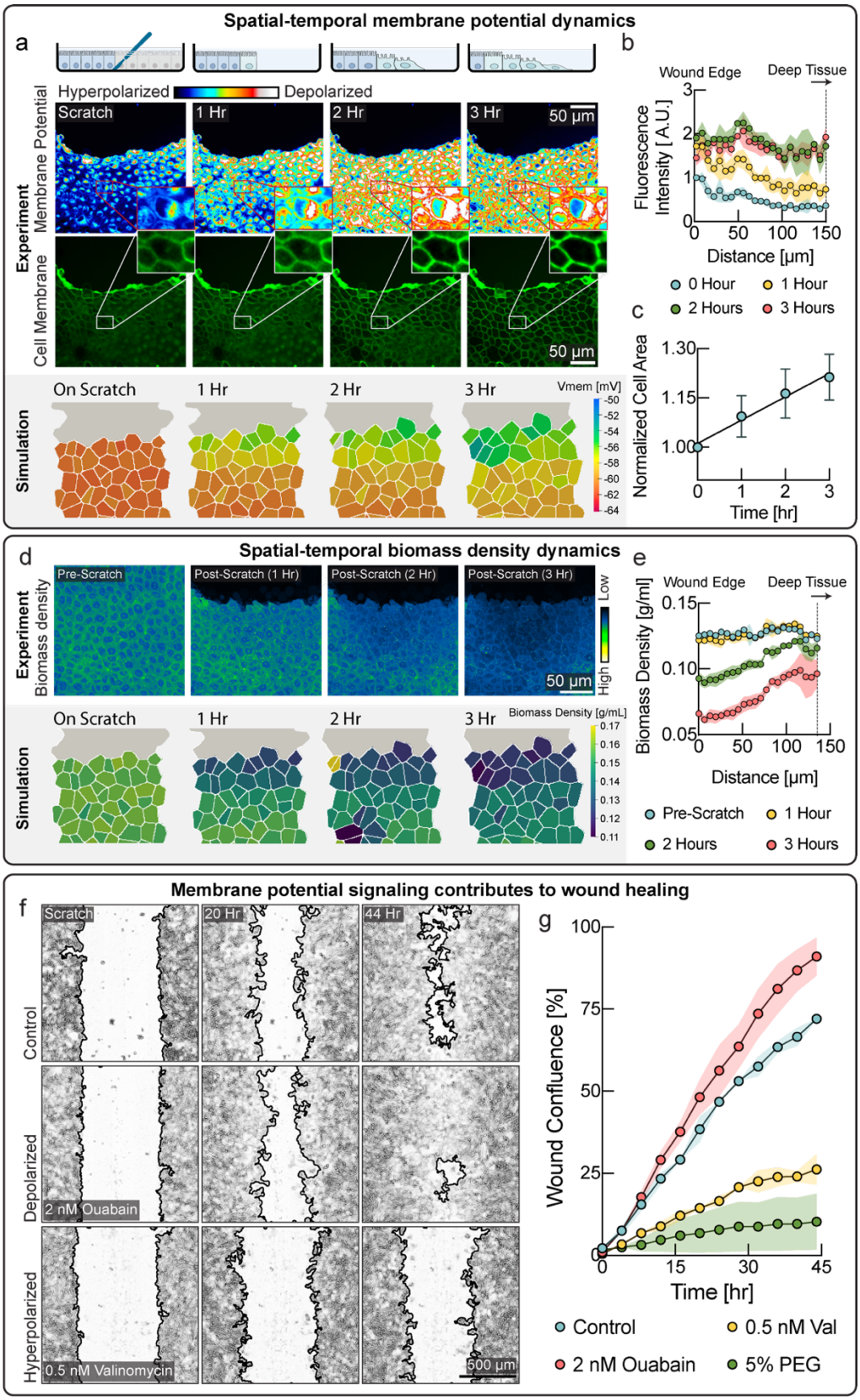

Figure 3: A mechanically induced depolarization wave enhances wound healing. a, *Upper panel: Cells progressively depolarize with time after scratch wound formation. Cells immediately*

next to the wound depolarize earlier and the depolarization wave propagate deeper in the tissue as time progresses. Membrane potential was measured via the membrane potential dye DisBac. An increase in fluorescence intensity (color scale) represents depolarization. Lower panel: Area of cells close to the wound increases with time, indicative of mechanical. Lower panel: Membrane potential from the tissue simulation over the course of wound healing. ***b****, Quantification of membrane potential as a function of distance from scratch wound at different times.* ***c,*** *Quantification of cell area shows expansion of cells during wound healing.* ***d,*** *Upper panel****:*** *Biomass density via NoRI imaging over the course of wound healing. Lower panel: Biomass density from the tissue simulation over the course of wound healing.* ***e.*** *Quantification of cellular biomass density as a function distance from scratch wound at different times after wounding.* ***f,*** *Wound healing efficiency is modulated by changes in membrane potential. Representative microscopic images of control well, depolarizing drug treatment (ouabain) and hyperpolarizing drug treatment (valinomycin). Mild depolarization results in better wound healing, as compared to control. The improvement in wound healing speed was also found with treatment with other depolarizing drugs (Fig. S11). On the other hand, hyperpolarization severely disrupted wound healing.* ***g,*** *Quantification of wound area closed, plotted as a function of time. Depolarization resulted in faster wound healing (ouabain, red circles), as compared to the untreated control (cyan circles). Hyperpolarization (valinomycin, yellow circles) resulted in disruption of wound healing. Hyperpolarization via addition osmotic compression (5% PEG, green circles) had the same effect.*

Epithelial tissues often form critical barriers with the topological exterior, protecting animal bodies from infection. Wound healing therefore constitutes an essential epithelial function in response to injury, where mechanisms of tissue homeostasis are operating in high gear and mechanical regulation may play an important role. To test investigate the role of membrane potential in wound healing, we performed scratch wound assays on tissues of MDCK cells. Strikingly, we observed a wave of depolarization in the tissue that started at the wound's immediate edge and moved progressively deeper into the tissue over several hours (Fig. 3a, quantified in 3b). Depolarization at wound edges has been previously observed, but the mechanistic cause of this depolarization is poorly understood[26]. According to our model, a drop of biomass density due to mechanical stretching of the tissue could explain depolarization. Indeed, we observed an increase in cell area in the tissue indicative of mechanical stretch (Fig. 3a, middle & 3c), as cells became motile via the epithelial mesenchymal transition (Fig. S9) and moved into the wound area, pulling on the cell behind them. Using NoRI imaging, we quantified biomass density as a function of distance from the wound edge (Fig. 3d,e & Fig. S10). Remarkably, we observed a drop in biomass density that closely coincided with the depolarization wave. Indeed, the tissue simulation with the mechano-electro-osmotic model successfully recapitulates the temporal and spatial dynamics of biomass density and membrane potential during wound healing (Fig. 3a, d, lower panels).

We hypothesized that the physiological function of this wave of depolarization could be to upregulate motility forces and proliferation in cells that are not immediately adjacent to the wound edge, which would thereby speed up the wound healing process. Indeed, we observed both depolarization (Fig. 3a) and a drop-in biomass density (Fig. S9) in cell immediately adjacent to the wound, as they underwent the epithelial-mesenchymal transition. It is also known from traction force microscopy that motility forces of cells many cell rows away from the leading edge of the wound, generate most of the tissue tension resulting in wound closure[27]. Thus, according to this

hypothesis, cells at the immediate wound edge become motile first and move into the wound, which mechanically stretches cells in rows behind them. As this wave of mechanical stretch propagates deeper into the tissue, it causes a drop in biomass density, resulting in depolarization of membrane potential. Cells detecting stretch via membrane potential may upregulate motility, biomass production and proliferation to enhance wound healing.

We therefore tested if modulation of membrane potential directly affected the speed and efficiency of wound healing by applying depolarizing and hyperpolarizing drugs and quantifying wound healing speed. We used CHO cells instead of MDCK cells because MDCK tissues tended to detach entirely during scratch wounding when an automated scratch wounding device is used. Indeed, even low concentrations of hyperpolarizing drugs (valinomycin) dramatically slowed down wound healing (Fig. 3f, lower panel & Fig. 3g, yellow circles) as compared to the control. We established earlier that compression of cell by external osmolarity resulted in hyperpolarization of membrane potential (Fig. S4). Indeed, compression by external osmolarity (Fig. 3g, green circles & Fig. S11) phenocopies the effect of hyperpolarizing drugs. Even more remarkably, we also found that the efficiency of wound healing, could be boosted, becoming faster than wildtype tissues with the addition of depolarizing drugs (Fig. 3f, middle & Fig. 3g, red circles), as compared to the untreated control (Fig.3f, upper & Fig. 3g, cyan circles). Consistently, depolarization by other drugs showed a similar improvement of wound healing efficiency (Fig. S11). These data suggest that depolarizing cells with drug addition, provides them with a 'head start' to upregulate motility and proliferation, as compared to the control tissue, where depolarization is only triggered later, by stretching from other cells moving into the wound.

Recently, it was found that has several signal transduction pathways are modulated by membrane potential[3,28]. Our key observation that membrane potential is a direct readout of mechanical forces and tissue density puts these interactions in a physiological context. Beyond these recently discovered links, we wondered if membrane potential could more broadly play a role in signal transduction, specifically in pathways implicated in mechano-sensing such as YAP/TAZ and MAPK[7–12]. Indeed, we found that the nuclear-cytoplasmic localization of the Hippo pathway downstream effector YAP was continuously modulated by tissue density (Fig. 4a-c), consistent with classic observations that were thought to be mediated by adherence junctions[29]. We hypothesized that density dependent Hippo signaling could also be directly modulated by membrane potential. Remarkably, depolarization of membrane alone was sufficient to make YAP reenter the nucleus in highly confluent tissues and significantly shifted the nuclear to cytoplasmic YAP ratio (Fig. 4d) to levels comparable to the YAP ratio in cells at low confluence.

The observed regulation of YAP by membrane potential is easily understood from a physiological perspective in the context of our observations (Figs. 1-3). Because nuclear YAP localization promotes growth and cell cycle progression [30], YAP is in the nucleus in depolarized cells, signaling low tissue density, when cells need to proliferate to repair the tissue. On the other hand, YAP exits the nucleus in cells with polarized membrane potential, indicating high tissue densities, stopping proliferation when growth is not needed.

Next, tested the effect of membrane potential on MAP kinase pathways. We found that depolarization was sufficient to significantly shifty the nuclear-cytoplasmic localization of both p-p38 and p-Jnk in high density tissues (Fig. 4e,f), in the opposite direction as YAP localization.

Activation of these pathways at high tissue density may promote tissue homeostasis by suppressing proliferation, promoting autophagy, or inducing apoptosis or cell extrusion with sustained activation[31,32]. Finally, we also check the dependence of SRC signaling on membrane potential. Indeed, we found that depolarization strongly increased levels of phosphorylated SRC, while hyperpolarization strongly repressed them (Fig. 4j). This modulation of SRC was independent of the mechanism of action of these drugs, suggesting that rather than emerging from specific drug interactions, SRC signaling is directly modulated by membrane potential. SRC activation in depolarized conditions, signaling low tissue density or a wound, can activate proliferation and motility. Our findings, in combination with previously established interactions[3,28,33–37] , reveal a membrane potential mediated mechano-transduction pathway (Fig. 4k). The downstream cellular response elicited by this signal transduction cascade is consistent with the role of membrane potential in tissue homeostasis that we uncovered in Figs. 1-3. It is highly likely that parallel signaling routes of mechano-transduction via membrane potential exist.

In conclusion, cellular mechano-transduction mediated by membrane potential is a strikingly elegant mechanism of tissue homeostasis. Membrane potential conveys the mechanical state of the cell even in the absence of active regulation or active transport. Therefore, we think that regulation by membrane potential may have been among the first homeostatic mechanisms to emerge in multi-cellular organisms. This regulatory role of resting membrane potential in confluent tissues may have contributed to the evolution of excitable tissues. Moreover, the response of membrane potential to cellular compression may play a role in neuronal mechano-transduction. Finally, breakdown of homeostatic regulation mediated by membrane potential could drive tumor growth, e.g. via chronic cellular depolarization. This may explain the frequent occurrence of ectopic expression of neuronal ion channels in tumors[38] and the commonly observed phenotype of depolarized resting membrane potential in cancer cells[39].

Acknowledgements

We would like to thank Peter Sorger and Clarance Yapp for acess to their high content imaging systems. We thank Nikon imaging center at Harvard Medical School for help with all fluorescence imaging experiments. Specifically, we thank Jennifer Waters, Tally Lambert, Anna Payne-Tobin Jost for their valuable support with the microscopy. This project was supported by MIRA grant (5R35GM137895) and an HMS Junior Faculty Armenise grant to M.B. N.C.B was supported by following grants, National Science Foundation Graduate Research Fellowship Program and Systems, Synthetic, and Quantitative Biology Training grant award T32GM135014.

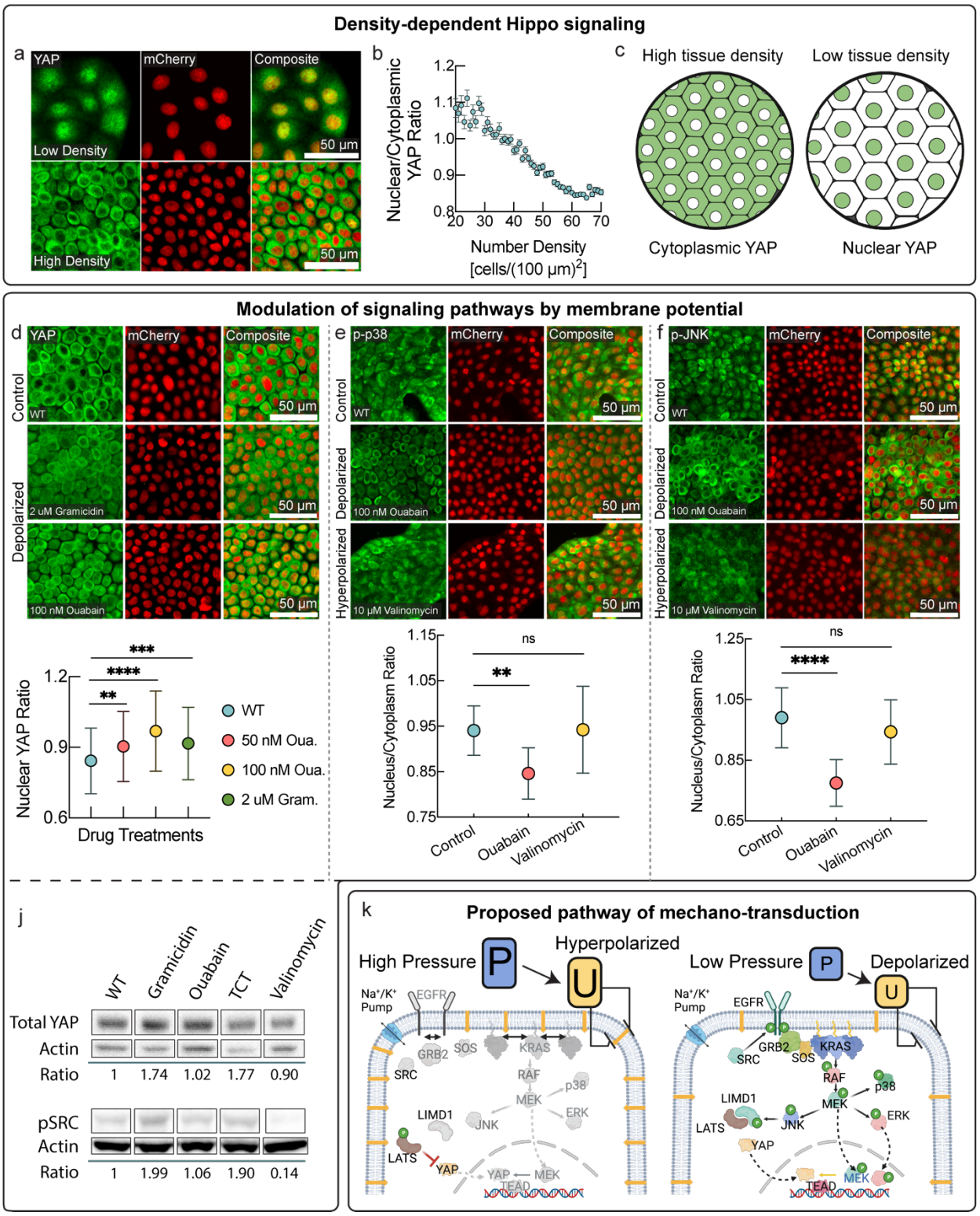

Figure 4 : Membrane potential mediated mechano-transduction pathways. a, *Localization of YAP via immunostaining in low density (top panel) and high density MDCK tissues (bottom panel).* ***b,*** *Quantification of nuclear to cytoplasmic YAP ratio as a function of cell number density.* ***c,*** *Schematic representation of YAP localization at different cell number densities. YAP is the Hippo pathway downstream effector that localizes to nucleus and promotes cell division in sub-confluent*

cells, whereas YAP is excluded from the nucleus in confluent cells, decreasing the rate of proliferation. ***d,*** *Depolarization promotes YAP re-entry in confluent MDCK cells. YAP is excluded from the cell nuclei in untreated confluent monolayers (top). YAP re-enters nuclei on depolarization by either gramicidin (middle) or ouabain (lower). Quantification of nuclear YAP ratio (plot below). YAP localization in depolarized, high-density tissues is comparable to sub-confluent cells (as quantified in panel b).* ***e,*** *Membrane potential dependence of localization of phosphorylated p38 from immunostaining. Phosphorylated p38 localizes to cell nuclei in dense tissues. Depolarization by ouabain resulted in nuclear exclusion of phosphorylated p38. Hyperpolarization by valinomycin resulted in uniform distribution of phosphorylated p38 in cell nuclei and cytoplasm. Nuclear to cytoplasmic ratio of phosphorylated p38 is quantified in plot below.* ***f,*** *Membrane potential dependence of localization of phosphorylated JNK from immunostaining. Depolarization via ouabain caused nuclear exclusion and increased cytoplasmic localization of phosphorylated JNK (middle), whereas the untreated control (top), as well as hyperpolarization via valinomycin (bottom) exhibited uniform distribution between nuclei and cytoplasm. Quantification of nuclear to cytoplasmic ratio of phosphorylated JNK shown in plot below.* ***j.*** *Top: Western blot showing increase in total cellular YAP caused by mild depolarization by either gramicidin, the gramicidin analog TCT, or ouabain. Conversely, mild hyperpolarization by valinomycin caused a slight decrease in total cellular YAP levels. Bottom: Western blot of phosphorylated SRC. Phosphorylated SRC levels increased with mild depolarization by either gramicidin or the gramicidin analog TCT. Conversely, hyperpolarization by valinomycin strongly reduced levels of phosphorylated SRC.* ***k,*** *Signaling routes of mechano-transduction via membrane potential. Mechanical pressure is directly reflected in membrane potential. EGFR and KRAS are directly exposed to the electric field across the plasma membrane due to membrane potential. KRAS has been shown to be modulated by membrane potential*[3,37]*. MAP kinases pathways are downstream from EGFR and KRAS. JNK in turn, can affect the localization of YAP via LIMD1.*

References

1. *Molecular Biology of the Cell: Reference edition, Band 1*. (2008).
2. Hille, B. Ion channels of excitable membranes. in (2001).
3. Zhou, Y. *et al.* Membrane potential modulates plasma membrane phospholipid dynamics and K-Ras signaling. *Science (1979)* **349**, 873–876 (2015).
4. Wang, Y. *et al.* Regulation of EGFR nanocluster formation by ionic protein-lipid interaction. *Cell Res* **24**, 959–976 (2014).
5. Coste, B. *et al.* Piezo1 and Piezo2 are essential components of distinct mechanically activated cation channels. *Science (1979)* **330**, 55–60 (2010).
6. Moroni, M., Servin-Vences, M. R., Fleischer, R., Sánchez-Carranza, O. & Lewin, G. R. Voltage gating of mechanosensitive PIEZO channels. *Nature Communications 2018 9:1* **9**, 1–15 (2018).
7. Chang, Y. C., Wu, J. W., Wang, C. W. & Jang, A. C. C. Hippo Signaling-Mediated Mechanotransduction in Cell Movement and Cancer Metastasis. *Front Mol Biosci* **6**, 157 (2020).
8. HuangFu, W.-C., Omori, E., Akira, S., Matsumoto, K. & Ninomiya-Tsuji, J. Osmotic Stress Activates the TAK1-JNK Pathway While Blocking TAK1-mediated NF- B Activation: TAO2 REGULATES TAK1 PATHWAYS. *Journal of Biological Chemistry* **281**, 28802–28810 (2006).
9. Lee, S.-H., Park, Y., Yoon, S. K. & Yoon, J.-B. Osmotic stress inhibits proteasome by p38 MAPK-dependent phosphorylation. *J Biol Chem* **285**, 41280–9 (2010).
10. Kishi, H. *et al.* Osmotic shock induces G1 arrest through p53 phosphorylation at Ser33 by activated p38MAPK without phosphorylation at Ser15 and Ser20. *J Biol Chem* **276**, 39115–22 (2001).
11. Messaoud, N. ben, Katzarova, I. & López, J. M. Basic Properties of the p38 Signaling Pathway in Response to Hyperosmotic Shock. doi:10.1371/journal.pone.0135249.
12. Niisato, N., Post, M., van Driessche, W. & Marunaka, Y. Cell Swelling Activates Stress-Activated Protein Kinases, p38 MAP Kinase and JNK, in Renal Epithelial A6 Cells. *Biochem Biophys Res Commun* **266**, 547–550 (1999).
13. Dupont, S. *et al.* Role of YAP/TAZ in mechanotransduction. *Nature* **474**, 179–183 (2011).
14. Panciera, T., Azzolin, L., Cordenonsi, M. & Piccolo, S. Mechanobiology of YAP and TAZ in physiology and disease. *Nat Rev Mol Cell Biol* **18**, 758–770 (2017).
15. Tyler, S. Epithelium--The Primary Building Block for Metazoan Complexity. *Integr Comp Biol* **43**, 55–63 (2003).
16. Oh, S. *et al.* Protein and lipid mass concentration measurement in tissues by stimulated Raman scattering microscopy. *Proc Natl Acad Sci U S A* **119**, e2117938119 (2022).
17. Park, H. *et al.* Three-dimensional refractive index tomograms and deformability of individual human red blood cells from cord blood of newborn infants and maternal blood. *https://doi.org/10.1117/1.JBO.20.11.111208* **20**, 111208 (2015).
18. Shin, S., Kim, K., Yoon, J. & Park, Y. Active illumination using a digital micromirror device for quantitative phase imaging. *Optics Letters, Vol. 40, Issue 22, pp. 5407-5410* **40**, 5407–5410 (2015).

19. Donnan, F. G. Theorie der Membrangleichgewichte und Membranpotentiale bei Vorhandensein von nicht dialysierenden Elektrolyten. Ein Beitrag zur physikalisch-chemischen Physiologie. *Zeitschrift für Elektrochemie und angewandte physikalische Chemie* **17**, 572–581 (1911).
20. Abdelfattah, A. S. *et al.* Bright and photostable chemigenetic indicators for extended in vivo voltage imaging. *Science (1979)* **365**, 699–704 (2019).
21. Eisenhoffer, G. T. *et al.* Crowding induces live cell extrusion to maintain homeostatic cell numbers in epithelia. *Nature* **484**, 546–549 (2012).
22. Goldman, D. E. POTENTIAL, IMPEDANCE, AND RECTIFICATION IN MEMBRANES. *J Gen Physiol* **27**, 37 (1943).
23. Eisenhoffer, G. T. & Rosenblatt, J. Bringing balance by force: live cell extrusion controls epithelial cell numbers. *Trends Cell Biol* **23**, 185–192 (2013).
24. Park, J. *et al.* Screening fluorescent voltage indicators with spontaneously spiking HEK cells. *PLoS One* **8**, (2013).
25. Burgstahler, R. *et al.* Confocal ratiometric voltage imaging of cultured human keratinocytes reveals layer-specific responses to ATP. *Am J Physiol Cell Physiol* **284**, (2003).
26. Chifflet, S. *et al.* Early and late calcium waves during wound healing in corneal endothelial cells. *Wound Repair and Regeneration* **20**, 28–37 (2012).
27. Trepat, X. *et al.* Physical forces during collective cell migration. *Nat Phys* **5**, 426–430 (2009).
28. Bartel, D. P., Sheng, M., Lau, L. F. & Greenberg, M. E. Growth factors and membrane depolarization activate distinct programs of early response gene expression: dissociation of fos and jun induction. *Genes Dev* **3**, 304–313 (1989).
29. Benham-Pyle, B. W., Pruitt, B. L. & Nelson, W. J. Mechanical strain induces E-cadherin–dependent Yap1 and β-catenin activation to drive cell cycle entry. *Science (1979)* **348**, 1024–1027 (2015).
30. Piccolo, S., Dupont, S. & Cordenonsi, M. The biology of YAP/TAZ: Hippo signaling and beyond. *Physiol Rev* **94**, 1287–1312 (2014).
31. Zeke, A., Misheva, M., Reményi, A. & Bogoyevitch, M. A. JNK Signaling: Regulation and Functions Based on Complex Protein-Protein Partnerships. *Microbiol Mol Biol Rev* **80**, 793 (2016).
32. Maik-Rachline, G., Lifshits, L. & Seger, R. Nuclear P38: Roles in Physiological and Pathological Processes and Regulation of Nuclear Translocation. *International Journal of Molecular Sciences 2020, Vol. 21, Page 6102* **21**, 6102 (2020).
33. Kapoor, A. *et al.* Yap1 Activation Enables Bypass of Oncogenic Kras Addiction in Pancreatic Cancer. *Cell* **158**, 185–197 (2014).
34. Zhang, W. *et al.* Downstream of Mutant KRAS, the Transcription Regulator YAP Is Essential for Neoplastic Progression to Pancreatic Ductal Adenocarcinoma. *Sci Signal* **7**, (2014).
35. Xu, H. *et al.* MEK nuclear localization promotes YAP stability via sequestering β-TrCP in KRAS mutant cancer cells. *Cell Death Differ* **26**, 2400–2415 (2019).
36. Codelia, V. A., Sun, G. & Irvine, K. D. Regulation of YAP by Mechanical Strain through Jnk and Hippo Signaling. *Current Biology* **24**, 2012–2017 (2014).

37. Rosen, L. Membrane depolarization and calcium influx stimulate MEK and MAP kinase via activation of Ras. *Neuron* **12**, 1207–1221 (1994).
38. Li, M. & Xiong, Z. G. Ion channels as targets for cancer therapy. *Int J Physiol Pathophysiol Pharmacol* **3**, 156 (2011).
39. Yang, M. & Brackenbury, W. J. Membrane potential and cancer progression. *Front Physiol* **4**, (2013).